



Development of a Griffin model of the advanced test reactor

February 2025

Changing the World's Energy Future

Mark D DeHart, Khang Nguyen, Yaqi Wang, Joshua Thomas Hanophy



DISCLAIMER

This information was prepared as an account of work sponsored by an agency of the U.S. Government. Neither the U.S. Government nor any agency thereof, nor any of their employees, makes any warranty, expressed or implied, or assumes any legal liability or responsibility for the accuracy, completeness, or usefulness, of any information, apparatus, product, or process disclosed, or represents that its use would not infringe privately owned rights. References herein to any specific commercial product, process, or service by trade name, trade mark, manufacturer, or otherwise, does not necessarily constitute or imply its endorsement, recommendation, or favoring by the U.S. Government or any agency thereof. The views and opinions of authors expressed herein do not necessarily state or reflect those of the U.S. Government or any agency thereof.

Development of a Griffin model of the advanced test reactor

Mark D DeHart, Khang Nguyen, Yaqi Wang, Joshua Thomas Hanophy

February 2025

**Idaho National Laboratory
Idaho Falls, Idaho 83415**

<http://www.inl.gov>

**Prepared for the
U.S. Department of Energy
Under DOE Idaho Operations Office
Contract DE-AC07-05ID14517**

Development of a Griffin Model of the Advanced Test Reactor

Khang H. N. Nguyen^a, Mark D. DeHart^b, Joshua T. Hanophy^b, Yaqi Wang^b

^a*Department of Nuclear Engineering, North Carolina State University, P.O. 2500
Stinson Dr, Raleigh, 27607, NC, USA*

^b*Reactor Physics Methods and Analysis Department, Idaho National Laboratory, 2525
Fremont Ave, Idaho Falls, 83415, ID, USA*

Abstract

In the pursuit of a higher fidelity deterministic simulation capability of the Advanced Test Reactor, it is important to have a fast yet accurate deterministic neutronics model. To achieve this, we employed an advanced two-step method. The first step involves generating homogenized cross sections using OpenMC, a cutting-edge Monte Carlo neutron transport code. OpenMC offers excellent modular capabilities, allowing for easy component integration and flexibility in incorporating new designs into the model. The second step involves deterministic transport calculations, which are performed using Griffin, a reactor physics application based on the Multiphysics Object-Oriented Simulation Environment (MOOSE). To ensure the accurate spatial resolution and assignment of material cross sections, a Cubit-generated mesh for the Advanced Test Reactor is utilized as an intermediate step between the OpenMC and Griffin models; Griffin utilizes the mesh for its finite element solution, while OpenMC material identifications are written to the mesh file to be used in Griffin material assignments. Additionally, a Python-based script converts the cross sections generated by OpenMC into the ISOXML format required by Griffin. Initial comparisons using the Griffin diffusion solver indicated good agreement between the neutron multiplication factors obtained from the standalone OpenMC model and the Griffin model, with differences of less than 10 pcm in the 2D geometry configuration; it was later determined that this agreement was likely due to compensating effect and was more likely on the order of -700 pcm relative to the OpenMC solution. However, in three-dimensional calculations, an unacceptably large error (almost 8,000 pcm) was found in the Griffin solution with the diffusion solver. Sub-

sequent calculations using Griffin’s discrete ordinates solver demonstrated substantially improved agreement, within 116 pcm of the OpenMC solution used to generate the cross sections for Griffin. Building on this capability, future work will seek to perform more detailed validation calculations. The ultimate goal is to evaluate both transient and multiphysics simulations of the reactor.

Keywords:

Griffin, OpenMC, Advanced Test Reactor, ATR, Deterministic, Monte Carlo,

1. Introduction

The Advanced Test Reactor (ATR), located at Idaho National Laboratory (INL), is a 250 MWth high-flux test reactor with a variety of missions, including the accelerated testing of nuclear fuel and other materials in a very high neutron flux environment and medical and industrial isotope production. ATR construction began in November 1961 and was completed in late 1965. Fuel loading commenced in 1967, core testing was completed in 1969, and finally, full power operation was achieved in August 1969.

Simulation and modeling play a crucial role in various aspects of ATR operations, including experiment design, fuel cycle management, and core experiment safety analysis. Experiment design and analysis for the ATR typically involve sophisticated three dimensional (3D) Monte Carlo analysis, typically utilizing the well-known continuous-energy (CE) Monte Carlo N-Particle Transport version 5 (MCNP5) code [1]. The two dimensional (2D) deterministic neutron transport code HELIOS [2] is currently used for core operations (fuel loadings, safety limits support, etc.) [3]; although, another 3D Monte Carlo software is being evaluated to assume this role in the future. Nonetheless, in this report, we present a contemporary two-step method for modeling the ATR, aiming to develop an appropriate computational mesh, a new cross-section generation approach and a 3D deterministic solution for neutron fluxes and reaction rates. Although current work is limited to demonstration of the ability single-physics (neutronics) to simulate the ATR with OpenMC and Griffin, future work plans to demonstrate that this set of tools will provide a powerful multiphysics analysis capability with substantial flexibility in updating new designs or experiments. This process consists of a workflow involving the Monte Carlo code OpenMC [4], the

meshing tool Cubit [5], and the reactor multiphysics application Griffin [6], which is built on the Multiphysics Object-Oriented Simulation Environment (MOOSE) framework [7]. OpenMC serves as a standalone analysis and verification tool that can be used to generate appropriately weighted multigroup (MG) cross sections for use by Griffin to solve the neutron transport problem. A computational mesh generated with Cubit [5] provides a spatial mesh for Griffin finite element analysis and assigns *blocks* (spatial regions) that correspond to the cross section generation regions defined in the OpenMC model. These data are then processed into the ISOXML library. The Griffin model connects the two by assigning OpenMC material names to the corresponding blocks in the input mesh. The overall process of developing the ATR model is depicted in Figure 1.

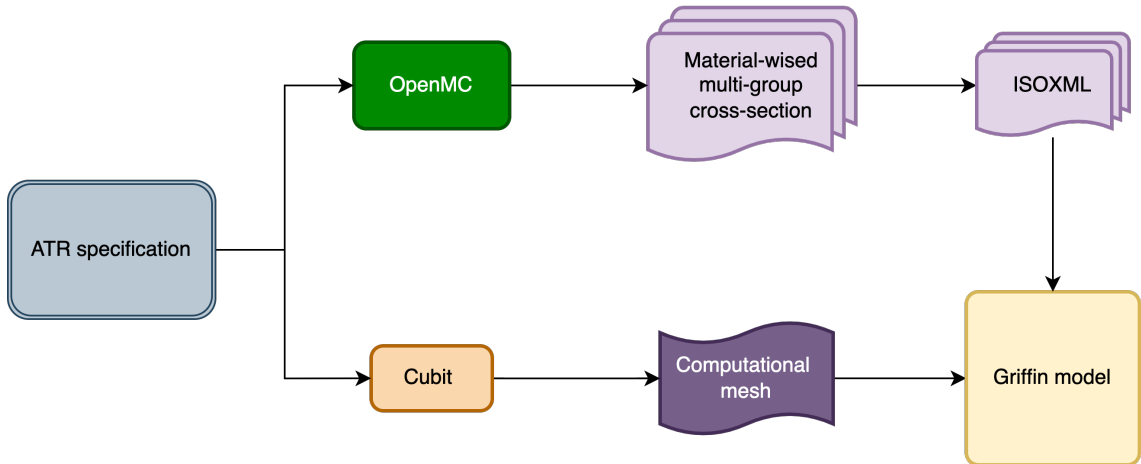


Figure 1: Workflow for ATR modeling with Griffin.

In this workflow, the OpenMC ATR model is developed based on the detailed core description available in the International Handbook of Evaluated Reactor Physics Benchmark Experiments (IRPhE) benchmark specification for the ATR [8]. In this benchmark specification, cooling channels in reflector and control drums are homogenized into the beryllium regions; regions above and below the active fuel length are also homogenized with appropriate homogenized materials provided in the benchmark specifications. The OpenMC model of this simplified benchmark specification is used to produce appropriately weighted multigroup cross section written in Extensible Markup Language (XML) format [9]. These cross sections are then converted

to Griffin’s ISOXML format (described in [10]). Meanwhile, using Cubit and its built-in Python scripting capabilities [5], a computational mesh is generated in which material assignments are made corresponding to the material identification numbers assigned in OpenMC. Finally, a Griffin model is executed using the cross-section data from OpenMC and the mesh generated by Cubit. This process is completed by comparing the OpenMC model to the published benchmark eigenvalue and comparing the Griffin results with the OpenMC results from which cross sections were obtained. In this work, both 2D (axially infinite) and 3D (based on the benchmark) calculations are performed.

This paper first introduces the ATR and the model used in this study and then gives an overview of the computer codes used in this work. Preliminary results using the ATR model are in the following section. Finally, this paper discusses the improved 3D results obtained using a higher order transport model. Through this process, we demonstrate our novel two-step approach that demonstrates the potential to enhance the efficiency and flexibility of ATR analyses by providing for the global accuracy of a deterministic transport solution. In future work, both steady-state and transient multiphysics analyses will be performed using the code coupling capabilities of Griffin inherited from the MOOSE framework.

2. Computer Codes

2.1. *OpenMC*

OpenMC is an open-source, community-developed Monte Carlo neutron and photon transport simulation code from the Massachusetts Institute of Technology [4]. It supports large-scale nuclear system simulations using high-performance computational systems, efficiently scaling to over 100,000 processors. OpenMC can handle models built with either constructive solid geometry or computer-aided design and supports both continuous-energy and multigroup transport. Continuous-energy data is based on Hierarchical Data Format Version 5 (HDF5) [11], generated from ACE-format files by NJOY2016 [12]. Its Python-based API allows for automated generation of input files.

Accurate multigroup cross sections require precise neutron flux determination, which is challenging due to the complex energy structure of cross sections, especially for heavier nuclides. While Monte Carlo methods like

OpenMC can accurately represent this energy dependence, they can be computationally demanding for conventional reactor analysis [9].

In this work, an OpenMC model of the ATR was constructed using an IRPhE benchmark specification, leveraging the OpenMC API and Python scripts. The model was validated against MCNP simulations, and multigroup cross sections were generated for each material for use in Griffin.

2.2. Cubit

Cubit [5] is a geometry and mesh generation software developed by Coreform, LLC and Sandia National Laboratories. It excels in reducing the time needed to generate large hexahedral meshes for complex geometries, supporting both 2D and 3D meshes for finite element analysis and computational fluid dynamics. Cubit includes various meshing algorithms and automation tools to streamline the meshing process. It also features a Python API, facilitating rapid mesh generation and refinement.

In this work, Cubit’s API is used to create a finite element mesh and assign material cross sections from the OpenMC model, linking the spatial placement of materials with their corresponding cross sections for neutron transport calculations.

2.3. Griffin

In late 2019, INL and Argonne National Laboratory (ANL) jointly developed Griffin [6, 13], a MOOSE-based reactor multiphysics application. Griffin integrates capabilities from MAMMOTH/Rattlesnake (INL) [10, 14] and MC²-3/PROTEUS (ANL) [15, 16] to streamline nuclear multiphysics analysis, including steady-state and transient radiation transport, core performance, fuel depletion, and criticality calculations. It offers flexibility through uniform MOOSE syntax, dynamic linking of relevant physics, and a single point of execution.

Griffin performs neutron, photon, thermal radiation, and phonon transport calculations with six available discretization schemes. These include continuous and discontinuous finite element methods for spatial discretization, and diffusion, spherical harmonics (PN), and discrete ordinates (SN) methods for angular discretization. Multischeme calculations efficiently manage computing resources by applying different discretization schemes to subdomains.

The unstructured mesh framework in MOOSE makes Griffin versatile for various reactor analyses, directly accounting for thermal expansion effects.

It supports homogenization equivalence methods and integrates with other MOOSE-based multiphysics applications like Pronghorn, RELAP-7, Sockeye, and BISON. Griffin has been used to model diverse reactor designs, including pebble-bed, prismatic, molten-salt, sodium-cooled fast reactors, nuclear thermal propulsion systems, and experimental facilities. Although multiphysics simulations are not applied in the current work, future studies will leverage this capability.

3. APPROACH

All calculations reported herein were run on the Sawtooth supercomputer within INL’s High Performance Computing Cluster [17]. This resource facilitated the efficient execution of the long OpenMC simulations and the large, memory-intensive Griffin calculations necessary for this work.

As discussed earlier, this endeavor began with the development of two OpenMC models of the core. These models were used to perform checks against the results provided for independently developed MCNP models of the full 3D and 2D extrusion of the benchmark specification [18] along with the benchmark evaluation itself [8]. These two models were used to prepare weighted cross sections for 2D and 3D Griffin models. Note that, as a MOOSE-derived application, Griffin is dimension agnostic and can solve 1D, 2D, and 3D problems.

Since the results used for comparison to other simulations used data from the ENDF/B-VII.0 data library [19], all calculations reported in this work are based on cross sections produced based on this evaluation. In OpenMC, scattering treatments ($S(\alpha, \beta)$) were used for beryllium and hydrogen in H_2O , and all cross section were evaluated at 300 K. All OpenMC simulations used 500 batches of 10,000 neutrons per batch, with the first 50 batches used for source convergence then discarded; the adequacy of this number of histories was demonstrated by obtaining statistically identical Griffin results using 500,000 neutrons per batch.

3.1. OpenMC Model

In this step, we first modeled the ATR core using the geometry and materials specifications outlined in the ATR benchmark specification [8]. The objective of this step is to ensure the model’s accuracy and reliability, which is subsequently compared to reported results. Because 2D results are available in Reference [18] for both MCNP and HELIOS calculations, based on

the core mid-fuel-plane geometry, a 2D version of the model was developed as well. Because both MCNP and OpenMC are inherently 3D, both models simulated the core as axially infinite, with a segment height of 1.0 cm; reflective boundary conditions were applied to the top and bottom of this segment to simulate the axially infinite core.

OpenMC also computes and generates flux-weighted multigroup neutron cross sections for the various materials, which are required for the deterministic neutron transport calculation. The 3D benchmark specification for the ATR is comprised of 44 distinct materials, with material specifications provided as isotopic compositions. We used OpenMC to generate multigroup cross sections for each material and establish a reference solution for comparison.

Figure 2 provides a structured flowchart illustrating the process used for generating the input for OpenMC for the ATR model. This diagram serves as a visual guide of the organization of the creation of the input files required to build the OpenMC model with its Python API. The modular approach used in this process allows for better organizing and flexibility in handling various components of the model. Each component is separated into distinct modules, enabling users to conveniently input new designs, materials, or parameters to adapt the model for different scenarios. Therefore, it allows for the easy exploration of different configurations and scenarios to gain valuable insights and optimize ATR modeling performance according to specific needs. An x-y cross-sectional cut of the geometry generated by the OpenMC model is illustrated in Figure 3. An axial cut is shown later in Figure 5.

An 18-group cross-section specification is also defined in the core model, based on the CASMO 18-group library data provided in Reference [20]. The energy group structure assumed for this work is given in Table 1. Sensitivity studies later performed with the Griffin model showed that this group structure was optimal for this model, based on the various CASMO-based cross-section energy structures provided in [21].

3.2. Converting Cross Section to ISOXML Format

We developed a Python-based converter script to translate the HDF-5 format multigroup cross sections generated by OpenMC into the XML-based ISOXML format required by the Griffin reactor multiphysics code. The cross sections produced by OpenMC are not directly compatible with Griffin's input capabilities, necessitating a conversion utility. The conversion process is straightforward for all types of reaction cross sections except removal cross

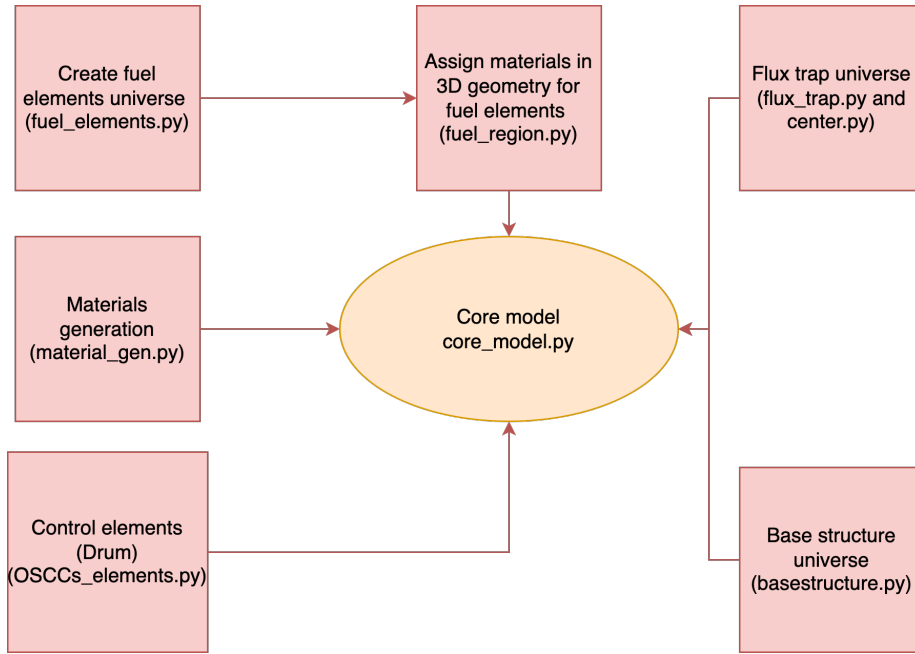


Figure 2: Input generation flow chart in OpenMC ATR model.

Table 1: Multigroup structure (The ascending order is from fast (group 1) to thermal (group 18)).

Group Index	Energy Range (eV)	Group Index	Energy Range (eV)
1	2.23E6 – 2.00E7	10	4.00E0 – 9.88E0
2	8.21E5 – 2.23E6	11	1.86E0 – 4.00E0
3	5.00E5 – 8.21E5	12	1.15E0 – 1.86E0
4	1.11E5 – 5.00E5	13	9.7E-1 – 1.15E0
5	9.12E3 – 1.11E5	14	6.25E-1 – 9.72E-1
6	5.53E3 – 9.12E3	15	2.80E-1 – 6.25E-1
7	1.47E2 – 5.53E3	16	1.40E-1 – 2.80E-1
8	1.60E1 – 1.49E2	17	5.80E-2 – 1.40E-1
9	9.88E0 – 1.60E1	18	00.E0 – 5.80E-2

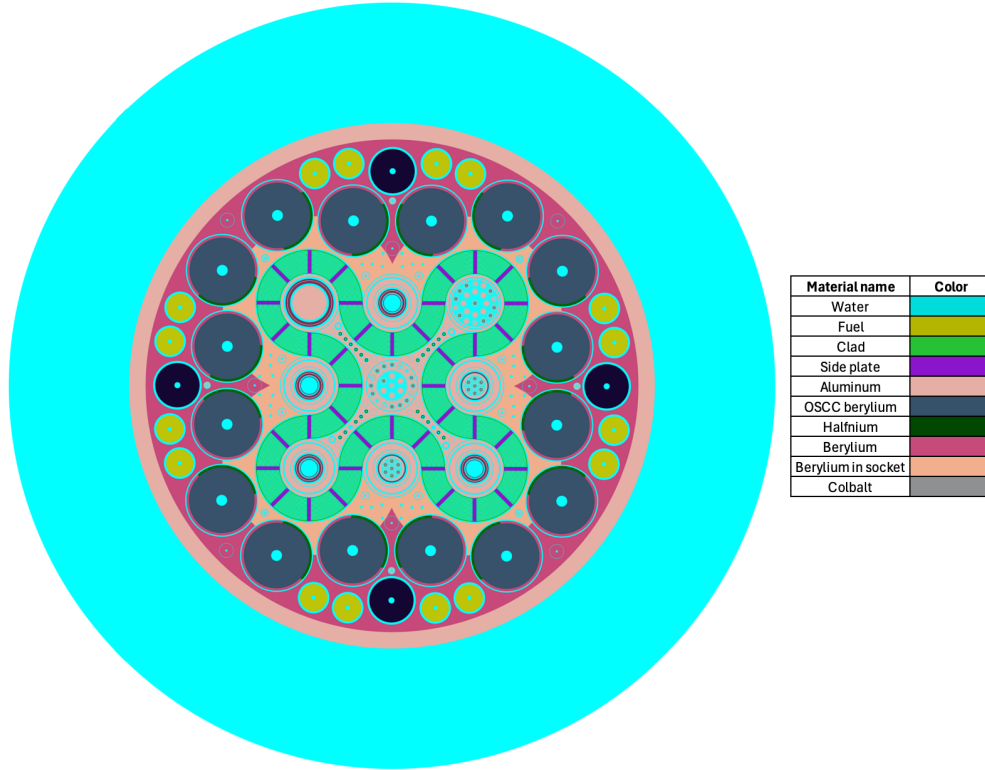


Figure 3: x-y cross-section view of the ATR generated by OpenMC (colored by material).

sections, which are used by diffusion calculations only and are calculated as in Equation [1](#). Currently, the converter is designed to produce cross sections for steady-state simulations in Griffin; though with modifications, it could be expanded to provide cross-section sets for transient or multiphysics simulations. When employing higher Legendre polynomial expansion orders, it's important to note that negative values may arise in the cross section of the scattering matrix. This phenomenon results from approximating the cosine of the scattering angle. The converter script facilitates using OpenMC-generated cross sections as input data for a core calculation with Griffin.

Removal cross sections for diffusion calculations are evaluated with

$$\Sigma_r^g = \Sigma_{ra}^g + \sum_{g'=1, g' \neq g}^G \Sigma_{ss}^{g \rightarrow g'} \quad (1)$$

where:

- Σ_r^g is the removal cross section of group g
- Σ_{ra}^g is the reduced absorption cross section of group g , which is defined as the difference between the absorption and production of neutrons due to (n,xn) reactions.
- $\sum_{g'=1, g' \neq g}^G \Sigma_{ss}^{g \rightarrow g'}$ represents the out-scattering cross section from group g .

3.3. Mesh Generation Using Cubit and the Mesh Extrusion Utility in Griffin

The ATR geometry in the benchmark specification is effectively variable in the x-y plane but uniform in the z direction; the material can change axially but the geometry does not. Hence, we created a 2D mesh of the ATR that could be extruded to three dimensions with appropriate axial material assignments. This mesh was generated using Cubit in a logical organization similar that used to create the OpenMC geometry model. The 2D mesh consists of 59 mesh blocks with triangular mesh elements and one block (outer water region) with quadrilateral mesh elements, which is illustrated in Figure 4. Each color represents a mesh block, however, the 19 fuel plates are too small to be seen in the figure. Each of the 59 blocks are assigned to one of the 44 materials specified in the IRPhE benchmark document; some of the same material was used in different blocks. Cubit uses blocks to group related sets of elements into a single entity. Each element in an element block must have the same element type and material assignment 5. The appropriate material identification number was assigned to each block in the scripting logic. A vacuum boundary condition was set on the exterior faces.

Using the MOOSE mesh extrusion tool, the 2D Cubit mesh is extruded to a 3D geometry using the axial discretization scheme provided in Table 2; here we selected the bottom of the active fuel to be 0.0. The scheme contains 13 axial blocks to account for axial changes in materials, as illustrated in Figure 5. This resulted in the 3D mesh expanding from the original 59 blocks in the 2D mesh to over 700 mesh blocks. The axial discretization introduces additional mesh blocks to more accurately represent the axial variation in geometry, materials, and cross sections within the ATR model, as illustrated in Figure 6. The growth in the number of blocks was a result of the extrusion process, which mapped each axial level to a new block ID. However, the same cross section was used for each axial block containing

the same material; future work will investigate computing and saving cross section for each axial region.

The mesh also serves to link the OpenMC-generated cross section to a Griffin model. The material-wise multigroup cross sections described in the previous section must be mapped onto the appropriate mesh blocks in Cubit. This allows Griffin to perform deterministic transport calculations using the Cubit-generated mesh and OpenMC-derived cross sections. The Python scripts used to generate the mesh also provide this mapping. The use of a mesh-based intermediate step facilitates the integration of the OpenMC and Griffin models; the mesh provides a mapping between the continuous spatial distribution of materials and cross sections in the OpenMC model and the discrete spatial representation of the Griffin transport solver. The same vacuum boundary condition was set on the exterior faces along with the top and bottom surfaces.

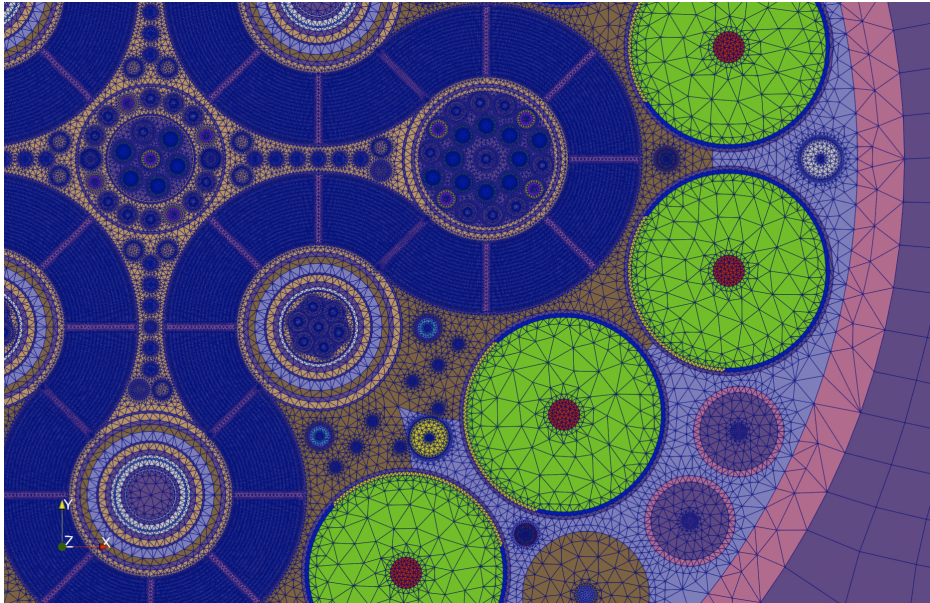


Figure 4: 2D mesh generated for the ATR using Cubit.

3.4. ATR Model in Griffin

The Griffin model was prepared with material assignments corresponding to the material names provided by OpenMC and ported to the ISOXML cross-section library and assigned to the appropriate blocks in the mesh file.

Table 2: Axial discretization for the 3D ATR model.

Axial Node	Height (cm)	Plane Begin (cm)	Plane End (cm)	# Subnode
1	7.62	147.32	139.7	1
2	2.54	139.7	137.16	1
3	10.16	137.16	127	1
4	3.175	127	123.825	1
5	1.905	123.825	121.92	1
6	7.62	121.92	114.3	1
7	109.22	114.3	5.08	11
8	2.0637	5.08	3.0163	1
9	3.0163	3.0163	0	1
10	1.905	0	-1.905	1
11	0.5895	-1.905	-2.54	1
12	5.715	-2.54	-8.255	1
13	12.74	-8.255	-20.995	1

Paths were provided to the Cubit-generated mesh and ISOXML cross-section file. The eigenvalue executioner was specified, and the continuous finite element method (CFEM) diffusion option was selected as the transport system solution scheme; this applies the CFEM to discretize the Griffin diffusion solver, based on the weak form of the multigroup diffusion equation [10].

As noted earlier, two Griffin models were created; the first was a 2D model with 59 mesh blocks containing a subset of assigned materials (top and bottom materials not present in this model). The second model, based on the first, included the mesh extrusion input and assigned materials to the mesh for each axial and radial block. The input was expanded to read the full set of materials from the corresponding ISOXML library and to assign materials to the correct blocks from the 3D mesh.

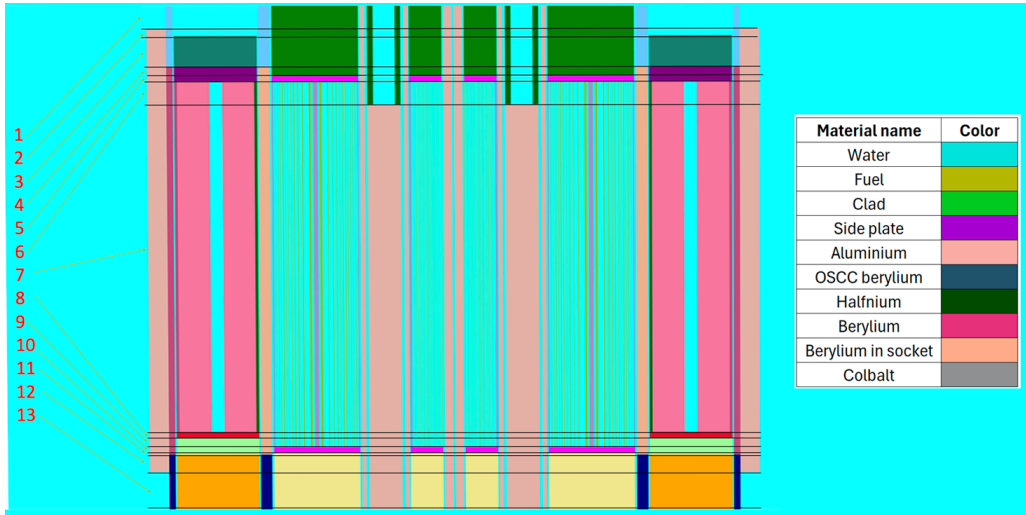


Figure 5: Axial node indexing scheme for ATR (colored by material).

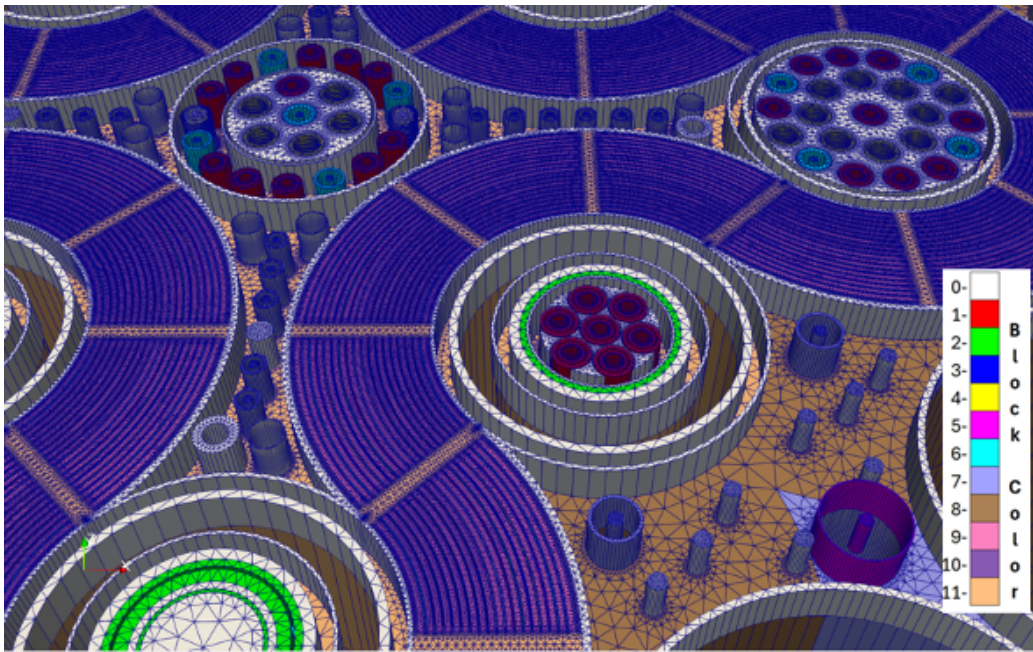


Figure 6: 3D mesh generated for the ATR using the extruded mesh generator in Griffin.

4. RESULTS

Because this process involves the two-step process for generating cross sections with OpenMC prior to using those cross sections in a Griffin transport calculation, we will examine each step separately, to be able to focus on the evaluation of each set of calculations. Section 4.1 describes the results obtained using 2D and 3D models of the ATR with OpenMC, comparing them to reference solutions. Clearly, cross sections generated using an incorrect model will yield incorrect results. In Section 4.2, we perform mesh convergence studies to obtain a spatially converged mesh. We then evaluate quadrature orders and scattering approximations to determine minimum acceptable values using the faster running 2D model, while using the OpenMC results as a reference solution. This process yields an optimized 3D ATR model for Griffin simulations.

4.1. OpenMC Modeling Results

In this section, we compare computed multiplication factors for 2D and 3D models. We then compare computed fuel element powers to experimentally measured values to understand potential differences in spatial solutions.

4.1.1. Comparison of Multiplication Factors

Once both the 2D and 3D OpenMC models had been developed, we conducted a confirmatory process to ascertain the accuracy of the OpenMC model relative to an MCNP model of the same configuration. This involved comparing the computed neutron multiplication factor with the values reported in [18], based on the the ATR benchmark [8]. The results exhibit a high degree of agreement. Table 3 provides a comparison of the results of a 2D (axially infinite) OpenMC model to those obtained using a 2D MCNP model, along with a deterministic 2D HELIOS solution. Differences are referenced to the MCNP solution. Agreement is within ± 132 pcm for all models, a little larger than might be desired. The examination of reaction rates studied in Section 4.1.2 may explain the differences between MCNP and OpenMC reasons for this difference.

Table 4 compares the results of the benchmark specification model to those of the MCNP5 and OpenMC calculations for the full 3D calculation. Here note that the reported datum for the actual ATR measurement is the critical configuration; therefore, the experimental value of k_{eff} was 1.0000 (uncertainty unknown). In the benchmark model, the assessed total bias uncertainty from the model simplifications was found to be -0.0018 ± 0.0010 . An

Table 3: Neutron multiplication factor comparison for 2D models.

Case	k_{eff}	Standard Deviation	Difference (pcm)
MCNP 2D [18]	1.03591	0.00014	—
HELIOS 2D [18]	1.03723	—	132
OpenMC 2D	1.03471	0.00002	-131

assessment of modeling uncertainties found a total uncertainty of ± 0.0033 . Therefore, the value of k_{eff} and uncertainty for the benchmark specification is 1.0018 ± 0.0035 [8]. Hence, 68% of simulations should fall in 0.9983–1.0116. Clearly both Monte Carlo results are within the range and are in very close agreement, within 3 pcm of each other.

The justification for these bias and uncertainty values are detailed in Section 3 of Reference [8]. They are largely a result of homogenization of details above and below the core and OSCCs, homogenization of cooling holes into larger regions (e.g., OSCCs and capsule plugs) and some geometric approximations (gear-shaped neck shims are approximated as equivalent cylinders, as was done for four square holes). However, the bias and uncertainties also result from potential errors in assumed compositions and from the cross section library used.

Table 4: Neutron multiplication factors for benchmark reference and 3D models.

Case	k_{eff}	Standard Deviation	Difference (pcm)
Benchmark Model [8]	1.0018	0.0035	—
MCNP [18]	0.99935	0.00014	245
OpenMC	0.99932	0.00002	248

4.1.2. Comparison of Reaction Rates Across the Core

Because the core eigenvalue is a global parameter, it does not capture spatial distributions, such as the distribution of reaction rates across the core. To this end, Table [5] provides a normalized fission power comparison each of the 40 fuel elements in the 3D models. Columns 2–4 provide measured data reported for fission wire averages within each fuel element in the core [8], OpenMC-calculated powers, and MCNP-computed powers

(also from Reference [8]), respectively. The last three columns compare the relative errors between OpenMC calculations and measured data, MCNP calculations and measured data, and OpenMC to the reference MCNP calculation. While uncertainties are not reported for the measured powers nor for the MCNP results, the OpenMC results are well converged and have an average 1σ uncertainty of 5.80×10^{-6} (0.0238%), ranging from 4.26×10^{-6} (0.0193%) to 6.85×10^{-6} (0.0320%). Table [6] demonstrates a good level of agreement between the OpenMC model and lobe powers (fuel element numbers associated with each lobe are also provided in this table); here the average 1σ uncertainty for the OpenMC results is 4.64×10^{-6} (0.0238%), ranging from 4.22×10^{-6} (0.0200%) to 4.83×10^{-6} (0.0260%). The relative differences lie between 14.0% and 8.0% when comparing with measurement results and MCNP simulation results, respectively, well outside the statistic uncertainties of the calculations. Both codes are found to underpredict powers in the southeast lobe, but OpenMC shows a larger difference.

These 3D results are also illustrated in Figure [7]. Both the table and plot show good agreement. However, there seem to be trends in the differences between MCNP and OpenMC. To examine this more closely, the difference between OpenMC and MCNP (relative to MCNP) is shown in Figure [8]. The figure shows that OpenMC tends to trend low in the SE lobe region and offsets with higher power predictions in the opposite northwest lobe region. This may be a result of an OpenMC modeling difference relative to MCNP in one of those lobes. However, the results provided earlier in Tables [3] and [4] seem to indicate a difference in radial solutions in 2D models that is diminished when the axial component is introduced in the 3D model.

4.2. Griffin Modeling Results

4.2.1. 2D Diffusion Models and Mesh Refinement

With general confidence in the overall spectrum produced in the OpenMC model, we generated multigroup cross sections using the approach described in Section [3.1] from both 2D and 3D models to use with the appropriate Griffin solution. The multigroup cross section exhibits a maximum uncertainty of 0.05% when utilizing the simulation option described in Section [3]. We then converted those cross sections to the ISOXML format used by Griffin, using the approach described in Section [3.2]. We started with the 2D OpenMC model to allow us to work with a simpler finite element mesh for Griffin. The 2D mesh discussed in Section [3.3] was used in a Griffin model to verify that Griffin could reproduce the OpenMC eigenvalue. The

Table 5: Normalized power distribution for fuel elements between OpenMC and MCNP models compared to that of measured data from [8]

Element No.	Measured	OpenMC	MCNP	% Rel. Err. (OpenMC-Meas.)	% Rel. Err. (MCNP-Meas.)	% Rel. Err. (OpenMC-MCNP)
1	0.0266	0.0279	0.028	4.89	0.36	-0.36
2	0.0247	0.0259	0.026	4.86	0.39	-0.38
3	0.0223	0.0231	0.0229	3.59	-0.87	0.87
4	0.0173	0.0177	0.0177	2.31	0.00	0.00
5	0.0136	0.0147	0.0146	8.09	-0.68	0.68
6	0.0145	0.0145	0.0145	0.00	0.00	0.00
7	0.0171	0.0179	0.018	4.68	0.56	-0.56
8	0.0243	0.0242	0.0246	-0.41	1.65	-1.63
9	0.0261	0.0264	0.0274	1.15	3.79	-3.65
10	0.0277	0.0281	0.029	1.44	3.20	-3.10
11	0.0307	0.0296	0.0305	-3.58	3.04	-2.95
12	0.0324	0.0292	0.0306	-9.88	4.79	-4.58
13	0.0296	0.0271	0.0288	-8.45	6.27	-5.90
14	0.0258	0.0223	0.0236	-13.57	5.83	-5.51
15	0.0206	0.0189	0.0199	-8.25	5.29	-5.03
16	0.0206	0.0191	0.0199	-7.28	4.19	-4.02
17	0.0258	0.0234	0.024	-9.30	2.56	-2.50
18	0.0296	0.029	0.0298	-2.03	2.76	-2.68
19	0.0324	0.0305	0.0314	-5.86	2.95	-2.87
20	0.032	0.031	0.0315	-3.13	1.61	-1.59
21	0.032	0.0317	0.0316	-0.94	-0.32	0.32
22	0.0322	0.0312	0.0311	-3.11	-0.32	0.32
23	0.0309	0.0297	0.0295	-3.88	-0.67	0.68
24	0.025	0.0246	0.0238	-1.60	-3.25	3.36
25	0.0196	0.0204	0.0199	4.08	-2.45	2.51
26	0.0202	0.0205	0.0197	1.49	-3.90	4.06
27	0.024	0.0252	0.0234	5.00	-7.14	7.69
28	0.0285	0.0303	0.0282	6.32	-6.93	7.45
29	0.0307	0.0313	0.0302	1.95	-3.51	3.64
30	0.0297	0.0309	0.0302	4.04	-2.27	2.32
31	0.0283	0.0297	0.0291	4.95	-2.02	2.06
32	0.0273	0.0284	0.0278	4.03	-2.11	2.16
33	0.0246	0.0269	0.026	9.35	-3.35	3.46
34	0.0203	0.0214	0.021	5.42	-1.87	1.90
35	0.0164	0.0174	0.0172	6.10	-1.15	1.16
36	0.0172	0.0173	0.0171	0.58	-1.16	1.17
37	0.0202	0.0212	0.0205	4.95	-3.30	3.41
38	0.0252	0.0257	0.0252	1.98	-1.95	1.98
39	0.0266	0.0275	0.0273	3.38	-0.73	0.73
40	0.0275	0.0284	0.0281	3.27	-1.06	1.07

initial highly refined mesh contained 1.68×10^6 elements. The OpenMC 2D model calculation yielded an eigenvalue of 1.03457 ± 0.00002 , with Griffin calculating 1.03471 for a -31 pcm difference. This and the following 2D calcu-

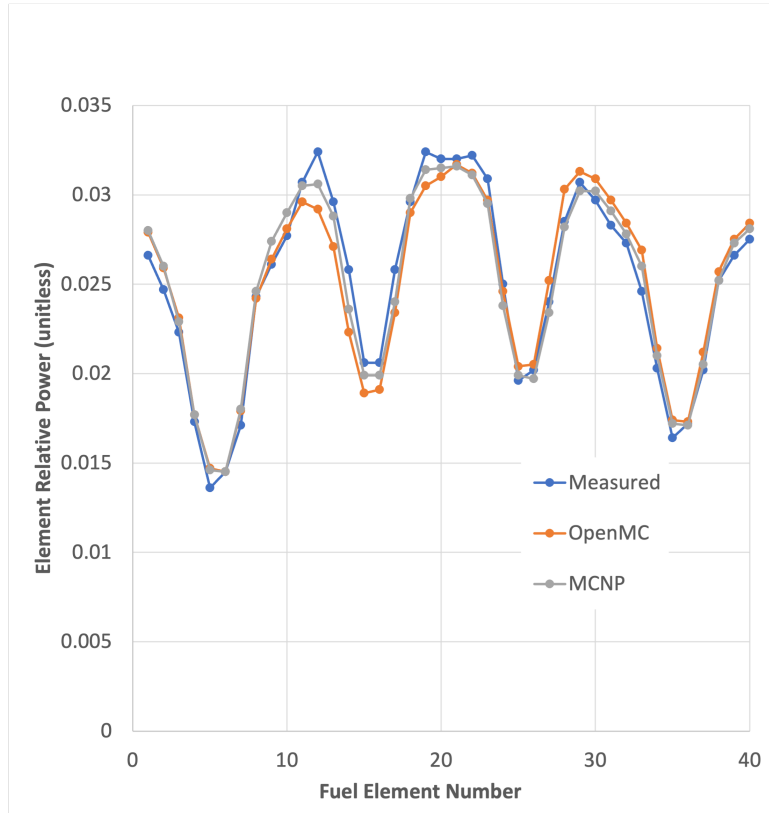


Figure 7: Comparison of measured and calculated relative powers using OpenMC and MCNP.

Table 6: Normalized power distribution by lobe.

Lobe No.	Lobe Fuel Elements	Measured	OpenMC	MCNP	% Rel. Err. (OpenMC-Meas.)	% Rel. Err. (MCNP-Meas.)	% Rel. Err. (OpenMC-MCNP)
NE	2-9	0.1599	0.1644	0.1658	2.80	3.68	-0.84
SE	12-19	0.2168	0.1995	0.2081	-7.99	-4.01	-4.14
NW	22-29	0.1778	0.1858	0.182	4.50	2.36	2.09
SW	32-39	0.2111	0.2132	0.2059	0.98	-2.46	3.53
Center	1, 10-11,20-21, 30-31, 40	0.2345	0.2373	0.2381	1.18	1.54	-0.35

lations were performed using the Griffin Continuous Finite Element Method (CFEM) diffusion solver. Note that at this point we performed the solution without using Griffin’s Super Homogenization (SPH) treatment [22]; that is planned for future work. Within the Griffin calculation, for the *Transport-Systems* input block, the following was specified for performing the diffusion

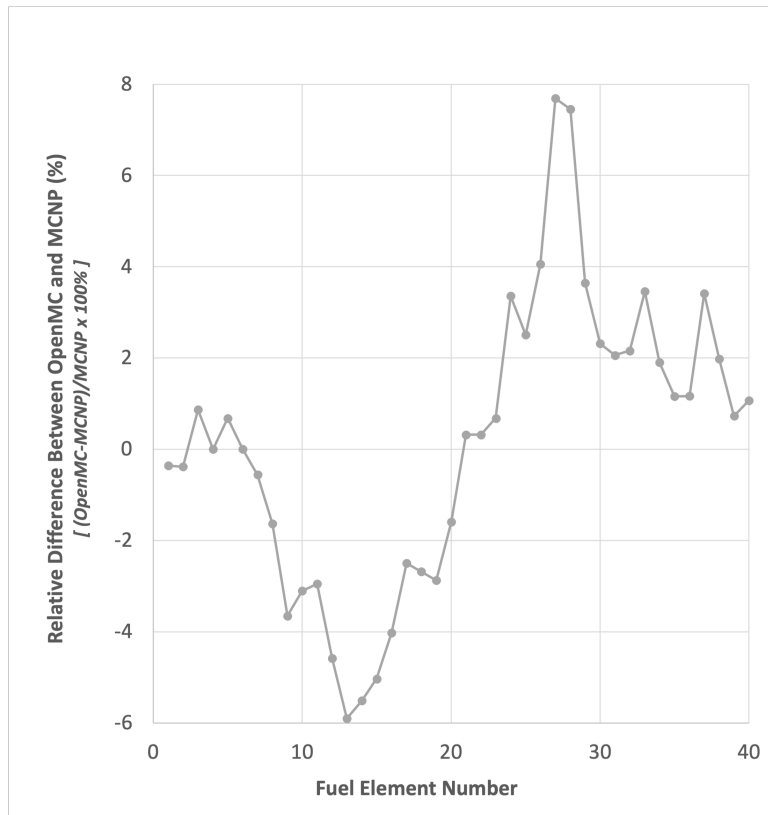


Figure 8: Differences between the calculated relative powers by OpenMC and MCNP by ATR element.

solution:

```
[TransportSystems]
  particle = neutron
  equation_type = eigenvalue
  G = 18
  VacuumBoundary = 1
  [diff]
    scheme = CFEM-Diffusion
    collapse_scattering = true
    fixed_jacobian = true
  []
[]
```

Meshing the ATR requires a very fine mesh in the fuel elements, some detail in the various flux traps, and lesser detail for the balance of the core. In developing meshing scripts, separate refinement factors were defined: one for the fuel, five representing five different kinds of flux traps, and another for the balance of the core. In addition, we determined that the mesh accuracy could be affected by the Cubit *trimesh surface gradation* factor. This parameter controls the growth of triangles where element size has been determined by bounding curves [5], so a variation of this parameter was also provided for in the ATR mesh scripting logic. By varying these factors we can develop a poor mesh with a large number of elements or an accurate mesh with much fewer elements. Judicial selection of the various parameters was required to reduce the size of the overall mesh to retain accuracy. A description of that process is outside the scope of this paper. However, we performed parametric studies to find the most accurate mesh structures for a given number of mesh cells.

Table 7: Neutron multiplication factor sensitivity to mesh size in the 2D ATR case.

Case	# Cells	Execute Time (m)	k_{eff}	Diff. (pcm)
1	1,680,482	11.33	1.034713	—
2	1,509,896	9.75	1.034691	-2.2
3	1,274,506	8.80	1.034672	-4.1
4	643,558	4.44	1.034619	-9.4
5	420,862	2.77	1.034615	-9.8
6	310,364	2.06	1.034618	-9.5
7	302,156	2.14	1.035426	71.3
8	287,096	2.09	1.037619	290.6

Given this approach, we then proceeded to conduct a 2D mesh sensitivity study by reducing the number of mesh cells to determine the relationship between mesh size and the neutron multiplication factor, with results provided in Table 7. The table provides execution times for each mesh size, showing a very linear relationship between mesh size and computational time. The simulations were performed utilizing 48 instances of MPI (message passing interface) on a single node on Sawtooth. At something on the order of 305,000 cells, the solution began to diverge from the higher order solution; changes in meshing parameters did not improve the solution at this point. The computational time using Mesh Example 6, with 310,364 cells (a fac-

tor of 5.4 reduction), was $5.5\times$ faster, with only around a 10 pcm difference in the neutron multiplication factor compared to the fine mesh. As noted above, further reducing the mesh size yielded increasing error; run time also increased slightly, or at best leveled off, with further mesh refinement.

Table 8 provides a direct comparison of the 2D OpenMC solution to the refined mesh Griffin 2D solution. Note that there was strong agreement between the 2D OpenMC and Griffin models. Comparing the fine mesh solution of 1.034713 from Griffin to the OpenMC 2D result of 1.03460, we find that the Griffin solution is only 11 pcm higher. We observe that reducing the mesh size reduces this difference, but we assumed that this is the result of offsetting error terms. Hence, a comparison to a lower order mesh solution would show a misleading higher level of agreement. When using OpenMC in

Table 8: Comparison of 2D k_{eff} between Griffin and the reference OpenMC solution.

Model	Neutron Multiplication Factor (k_{eff})	Dif. (pcm)
OpenMC 2D (CE mode)	1.03460 ± 0.00002	—
OpenMC 2D (MG mode)	1.04185 ± 0.00002	—
Griffin 2D (Diffusion)	1.03471	11 (CE) / -714 (MG)

MG mode, there is an approximately -700 pcm difference in the multiplication factor compared to the continuous energy calculation. Because the Griffin diffusion solution used the same MG cross sections, it should have been in closer agreement with the OpenMC MG simulation. This indicates likely compensating errors in the Griffin solution, and that the 11 pcm agreement was simply fortuitous.

We believe that the primary reason for the difference between OpenMC CE and MG solutions is that the cross sections were generated material-wise, i.e., averaged by the local flux in the material over all regions in which the material is found, which incorrectly weights cross sections. In future work, one possible solution would to use mesh-based cross sections; however, achieving accurate spatial effects would necessitate a highly detailed mesh, leading to high computational costs. Breaking up materials by region is a more feasible solution, but that is beyond the scope of this work.

4.2.2. 3D Griffin Models

The next step in this investigation was to extrude the model mesh to three dimensions, as described in Section 3.4. Here we used the mesh of Case 6 from Table 8 with 310,364 in two dimensions. Extruding using the 23 axial discretization scheme with 11 zones in the active fuel height, as shown in Table 2 and Figure 5, a 3D mesh was created with 7,138,372 computational cells. This model used all 59 material blocks; in moving to the 3D model, additional top and bottom structural materials and a reflector were added.

Using cross sections generated using the 3D OpenMC model, the same solver was used simulate the full core. However, this calculation yielded an eigenvalue of 0.92004. After reviewing the input specifications and the mesh generation process, we decided that the diffusion solver may not be sufficient for this 3D problem with its relatively coarse axial discretization. As shown in Table 9, the diffusion solution resulted in an almost -8000 error relative to OpenMC. However, recall that the ATR is a small core (1.2 m tall and approximately 100 cm across at the maximum radial extent). The thick beryllium radial reflector outside the core significantly reduces radial leakage. However, the top and bottom of the fuel regions are reflected primarily by water, resulting in more significant axial leakage. This flux gradient is a challenge to the diffusion equation for the applied axial discretization, requiring a higher order solution. Even with the 2D diffusion solution, the error is on the order of 700 pcm. Hence, we converted the model to a transport solution using Griffin's discontinuous finite element method (DFEM) S_N (discrete ordinates) solver with the following specification:

```
[Executioner]
  type = SweepUpdate
  verbose = true
  richardson_rel_tol = 1e-12
  richardson_abs_tol = 1e-8
  richardson_max_its = 50
  richardson_value = eigenvalue
  inner_solve_type = GMRes
  max_inner_its = 8
[]
[TransportSystems]
  particle = neutron
  equation_type = eigenvalue
  G = 18
  VacuumBoundary = '1 top bottom'
[sn]
```

```

    scheme = DFEM-SN
    family = MONOMIAL
    order = FIRST
    AQtype = Gauss-Chebyshev
    NPolar = 2
    NAzmth1 = 4
    NA = 2
  []
[]

```

The quadrature set uses two polar and four azimuthal angles per spatial octant and a scattering order of two. The calculation used twenty-four central processing units on each of 6 nodes on the INL cluster. The calculation was able to yield a much improved solution. Griffin calculated an eigenvalue of 1.0000; however, the solution required a large number of iterations to converge. To improve performance, we added Griffin’s coarse-mesh finite difference (CMFD) accelerator. This was accomplished by adding a 20×20 rectangular mesh in the x-y plane, also extruded to 23 axial regions, for a total of 9,200 coarse mesh cells. The original mesh was modified to add the coarse mesh data, and the MOOSE *Executioner* block was modified as shown here:

```

[Executioner]
  type = SweepUpdate
  verbose = true
  richardson_rel_tol = 1e-4
  richardson_max_its = 50
  richardson_value = eigenvalue
  inner_solve_type = GMRes
  max_inner_its = 8
  max_diffusion_coefficient = 10
  cmfd_acceleration = true
  coarse_element_id = coarse_element_id
  diffusion_eigen_solver_type = newton
  prolongation_type = multiplicative
  diffusion_prec_type = lu
[]

```

This calculation did indeed show performance gains, converging to essentially the same answer. In fact, while the Griffin (S_N) case required 50 Richardson iterations to converge, the Griffin (S_N with CMFD) only required 14 Richardson iterations. Table 9 provides the eigenvalue and timing results of the various 3D calculations, including run times. All cases were run using

Table 9: Comparison of 3D k_{eff} between Griffin and the reference OpenMC solution.

Model	Neutron Multiplication Factor (k_{eff})	Diff. (pcm)	Time (h)
OpenMC	0.99932 ± 0.00002	—	2.73
Griffin (diffusion)	0.92004	-7,807	0.48
Griffin (S_N)	1.000482	116	13.8
Griffin (S_N with CMFD)	1.000484	116	1.68

144 processors spread over 6 nodes, all using the same partitioned mesh, to allow for a direct comparison. Error is referenced to the OpenMC result, as this is the model that was used to generate the cross sections used in the Griffin calculations. Similar to Table 5, in Table 10 we also plot power distributions by element, here showing only Griffin and OpenMC results relative to measured data. Table 11 shows the same data combined for each of the lobes.

The S_N transport calculations are in very good agreement with the reference OpenMC calculation. Clearly, Griffin’s CMFD acceleration yielded a significant performance gain over the unaccelerated solution. Table 10 combined with Table 11 show that the 3D CMFD-accelerated Griffin solution is in agreement with the 3D OpenMC element powers generally with a magnitude of error of less than 1% in NW, SW and Center positions, but larger errors are seen in the NE and SE lobes, with the magnitude of the error on the order of 1.5%. This indicates an area for further study, nevertheless we believe that we have demonstrated the capability to model the ATR using a three-dimensional Griffin model with cross-section generation using OpenMC.

5. CONCLUSIONS AND FUTURE WORK

In this work, we created two OpenMC models of the ATR—a full 3D model based on the benchmark specification of Reference 8 and an axially infinite, effectively 2D version based on the geometry at the axial midplane of the fuel region. A comparison of neutron multiplication factors showed very good agreement with benchmark results. A comparison of power distributions in the 3D core models between MCNP and OpenMC shows a small variation in the power distribution, with MCNP closer to the measured data.

Table 10: Normalized power distribution for fuel elements between Griffin and OpenMC models compared to that of measured data from [8].

Element No.	Measured	OpenMC	Griffin	% Rel. Err. (OpenMC-Meas.)	% Rel. Err. (Griffin-Meas.)	% Rel. Err. (Griffin-OpenMC)
1	0.0266	0.0279	0.0281	4.89	5.51	0.61
2	0.0247	0.0259	0.0257	4.86	4.22	-0.60
3	0.0223	0.0231	0.0228	3.59	2.23	-1.30
4	0.0173	0.0177	0.0174	2.31	0.60	-1.66
5	0.0136	0.0147	0.0144	8.09	6.11	-1.82
6	0.0145	0.0145	0.0142	0.00	-1.77	-1.76
7	0.0171	0.0179	0.0175	4.68	2.28	-2.29
8	0.0243	0.0242	0.0236	-0.40	-2.68	-2.27
9	0.0261	0.0264	0.0264	1.15	1.25	0.11
10	0.0277	0.0281	0.0285	1.44	2.90	1.45
11	0.0307	0.0296	0.0301	-3.50	-1.84	1.82
12	0.0324	0.0292	0.0297	-9.80	-8.17	1.90
13	0.0296	0.0271	0.0278	-8.40	-5.98	2.70
14	0.0258	0.0223	0.0230	-13.50	-10.83	3.17
15	0.0206	0.0189	0.0195	-8.20	-5.33	3.19
16	0.0206	0.0191	0.0196	-7.20	-4.79	2.70
17	0.0258	0.0234	0.0235	-9.30	-9.03	0.31
18	0.0296	0.0290	0.0289	-2.00	-2.52	-0.49
19	0.0324	0.0305	0.0307	-5.80	-5.17	0.75
20	0.0320	0.0310	0.0313	-3.10	-2.32	0.84
21	0.0320	0.0317	0.0318	-0.90	-0.52	0.43
22	0.0322	0.0312	0.0313	-3.10	-2.84	0.28
23	0.0309	0.0297	0.0295	-3.80	-4.48	-0.61
24	0.0250	0.0246	0.0242	-1.60	-3.10	-1.51
25	0.0196	0.0204	0.0204	4.08	4.28	0.20
26	0.0202	0.0205	0.0205	1.49	1.67	0.19
27	0.0240	0.0252	0.0250	5.00	4.01	-0.93
28	0.0285	0.0303	0.0299	6.32	4.80	-1.41
29	0.0307	0.0313	0.0312	1.95	1.67	-0.27
30	0.0297	0.0309	0.0312	4.04	5.14	1.07
31	0.0283	0.0297	0.0297	4.95	5.00	0.06
32	0.0273	0.0284	0.0282	4.03	3.29	-0.70
33	0.0246	0.0269	0.0264	9.35	7.52	-1.66
34	0.0203	0.0214	0.0211	5.42	3.94	-1.40
35	0.0164	0.0174	0.0174	6.10	6.22	0.13
36	0.0172	0.0173	0.0173	0.58	0.67	0.10
37	0.0202	0.0212	0.0206	4.95	2.15	-2.66
38	0.0252	0.0257	0.0254	1.98	0.80	-1.15
39	0.0266	0.0275	0.0275	3.38	3.23	-0.14
40	0.0275	0.0284	0.0284	3.27	3.29	0.03

This difference will be studied in future work. Both OpenMC models were also used to generate 18-group cross sections, and a Python-based script con-

Table 11: Normalized power distribution by lobe for Griffin compared to measured and OpenMC results.

Lobe No.	Lobe Fuel Elements	Measured	OpenMC	Griffin	% Rel. Err. (OpenMC-Meas.)	% Rel. Err. (Griffin-Meas.)	% Rel. Err. (Griffin-OpenMC)
NE	2-9	0.1599	0.1644	0.1622	2.8	1.43	-1.34
SE	12-19	0.2168	0.1995	0.2027	-7.99	-6.48	1.64
NW	22-29	0.1778	0.1858	0.1840	4.5	3.47	-0.97
SW	32-39	0.2111	0.2132	0.2120	0.98	0.45	-0.53
Center	1, 10-11,20-21, 30-31, 40	0.2345	0.2373	0.2391	1.18	1.98	0.79

verted the OpenMC HDF5-based cross sections to the *ISOXML* format used by Griffin. Comparisons between the 2D standalone OpenMC model and the Griffin fine mesh model showed an 11 pcm difference in the neutron multiplication factor using the diffusion solver within Griffin. However, for the 3D geometry case, unsatisfactory results were obtained when diffusion was used; the 7,807 pcm difference suggested that either inadequate axial discretization is being used or a higher order transport model is required to achieve more accurate results. Using Griffin’s DFEM-SN solver, we find much better agreement, calculating 116 pcm higher than the reference solution.

Research is ongoing to better understand and improve on the 3D power distribution results relative to MCNP and measured data, to reduce the error in the Griffin 3D calculation, and to improve the simulation performance. One of the first steps will be to correct for minor volumetric approximations resulting from a meshed approximation to the curved surfaces. Future work will also seek to simplify the model by applying super-homogenization (SPH) factors to allow the homogenization of portions of the model to further reduce mesh size. This model will then be used to investigate the application of the model to enhance the simulation of in-core experiments. However, it is important to note that the ultimate application of the Griffin simulation of the ATR will be to perform multiphysics simulations. In particular, we are interested in simulating the multiphysics behavior of experiments being irradiated in an in-pile tube, where test conditions (pressure, temperature, etc.) can be substantially different from nominal ATR operating condition. In addition, the transient capabilities of Griffin will be used to perform a direct simulation of limiting accident conditions to determine if conservatism in operational safety limits can be reduced.

Acknowledgments

Griffin is under continuous development by a team of software developers at ANL and INL. We'd like to acknowledge the whole development team for their efforts. This multi-laboratory collaboration has been primarily funded since its inception by the U.S. Department of Energy Nuclear Energy Advanced Modeling and Simulation (NEAMS) program.

The authors would like to thank Mustafa Jaradat and Ishita Trivedi of INL for their assistance and insights into early phases of this work, and Yeon Sang Jung and Namjae Choi for technical assistance with the CMFD solver. We also wish to thank the ATR Experiment Engineering Division within the Advanced Test Reactor Directorate for providing the funding for Mr. Nguyen's internship at INL, during which much of this research was performed. In addition, we wish to acknowledge that this research made significant use of the resources of the High Performance Computing Center located at the Collaborative Computing Center and supported by the Office of Nuclear Energy of the U.S. Department of Energy and the Nuclear Science User Facilities under Contract No. DE-AC07-05ID14517. This manuscript has been authored by Battelle Energy Alliance, LLC under Contract No. DE-AC07-05ID14517 with the U.S. Department of Energy. The U.S. Government retains and the publisher, by accepting the article for publication, acknowledges that the U.S. Government retains a nonexclusive, paid-up, irrevocable, worldwide license to publish or reproduce the published form of this manuscript, or allow others to do so, for U.S. Government purposes.

References

- [1] J. E. Sweezy, T. E. Booth, F. B. Brown, J. S. Bull, R. A. F. III, J. T. Goorley, H. G. H. III, R. L. Martz, R. E. Prael, A. Sood, A. J. Zukaitis, R. C. Little, H. R. Trellue, M. C. White, M. B. Lee, S. M. Girard, MCNP - Version 5, Vol. I: Overview and Theory, Technical Report LA-UR-03-1987 (Revised 2/1/2008), Los Alamos National Laboratory, 2003. URL: [https://mcnp.lanl.gov/pdf_files/TechReport_2003_LANL_LA-UR-03-1987Revised212008\\$\\$SweezyBoothEtAl.pdf](https://mcnp.lanl.gov/pdf_files/TechReport_2003_LANL_LA-UR-03-1987Revised212008$$SweezyBoothEtAl.pdf).
- [2] C. A. Wemple, H. N. M. Gheorghiu, R. J. J. Stamm'ler, E. A. Villarino, Recent advances in the helios-2 lattice physics code, in: Proceedings of the International Conference on Reactor Physics, Nuclear Power: A Sustainable Resource, 2008.

- [3] S. E. Bays, C. B. Davis, P. A. Archibald, Upgrading limiting peak-power analysis techniques with modern validation and uncertainty quantification for the advanced test reactor, *Nuclear Technology* 201 (2018) 209–227. URL: <https://doi.org/10.1080/00295450.2017.1415091>, doi:[10.1080/00295450.2017.1415091](https://doi.org/10.1080/00295450.2017.1415091).
- [4] P. K. Romano, N. E. Horelik, B. R. Herman, A. G. Nelson, B. Forget, K. Smith, OpenMC: A state-of-the-art monte carlo code for research and development, *Annals of Nuclear Energy* 82 (2015) 90–97. URL: <https://doi.org/10.1016/j.anucene.2014.07.048>, doi:[10.1016/j.anucene.2014.07.048](https://doi.org/10.1016/j.anucene.2014.07.048).
- [5] Cubit, LLC, 2020, Coreform Cubit (Version 15.7) [Computer software], URL: <https://coreform.com/>.
- [6] Y. Wang, Z. M. Prince, H. Park, O. W. Calvin, N. Choi, Y. S. Jung, S. Schunert, S. Kumar, J. T. Hanophy, V. M. Labouré, C. Lee, J. Ortensi, L. H. Harbour, J. R. Harter, Griffin: A moose-based reactor physics application for multiphysics simulation of advanced nuclear reactors, *Annals of Nuclear Energy* 211 (2025) 110917. URL: <https://www.sciencedirect.com/science/article/pii/S0306454924005802>, doi:<https://doi.org/10.1016/j.anucene.2024.110917>.
- [7] A. D. Lindsay, D. R. Gaston, C. J. Permann, J. M. Miller, D. Andrš, A. E. Slaughter, F. Kong, J. Hansel, R. W. Carlsen, C. Icenhour, L. Harbour, G. L. Giudicelli, R. H. Stogner, P. German, J. Badger, S. Biswas, L. Chapuis, C. Green, J. Hales, T. Hu, W. Jiang, Y. S. Jung, C. Matthews, Y. Miao, A. Novak, J. W. Peterson, Z. M. Prince, A. Rovinelli, S. Schunert, D. Schwen, B. W. Spencer, S. Veeraraghavan, A. Recuero, D. Yushu, Y. Wang, A. Wilkins, C. Wong, 2.0 - MOOSE: Enabling massively parallel multiphysics simulation, *SoftwareX* 20 (2022) 101202. URL: <https://www.sciencedirect.com/science/article/pii/S2352711022001200>, doi:<https://doi.org/10.1016/j.softx.2022.101202>.
- [8] S. S. Kim, B. G. Schnitzler, Advanced Test Reactor: Serpentine Arrangement of Highly Enriched Water-Moderated Uranium-Aluminide

- Fuel Plates Reflected by Beryllium, ATR-FUND-RESR-001, International Handbook of Evaluated Criticality Safety Benchmark Experiments (2021). doi:[10.1787/110ba6fc-en](https://doi.org/10.1787/110ba6fc-en).
- [9] W. Boyd, A. Nelson, P. K. Romano, S. Shaner, B. Forget, K. Smith, Multigroup cross-section generation with the openmc monte carlo particle transport code, Nuclear Technology 205 (2019) 928–944. URL: <https://doi.org/10.1080/00295450.2019.1571828>. doi:[10.1080/00295450.2019.1571828](https://doi.org/10.1080/00295450.2019.1571828). arXiv:<https://doi.org/10.1080/00295450.2019.1571828>.
- [10] Y. Wang, S. Schunert, J. Ortensi, V. Laboure, M. DeHart, Z. Prince, F. Kong, J. Harter, P. Balestra, F. Gleicher, Rattlesnake: A MOOSE-based multiphysics multi-scheme radiation transport application, Nuclear Technology 207 (2021) 1047–1072. URL: <https://doi.org/10.1080/00295450.2020.1843348>. doi:[10.1080/00295450.2020.1843348](https://doi.org/10.1080/00295450.2020.1843348). arXiv:<https://doi.org/10.1080/00295450.2020.1843348>.
- [11] T. Jenness, Reimplementing the hierarchical data system using hdf5, Astronomy and Computing 12 (2015) 221–228. URL: <https://www.sciencedirect.com/science/article/pii/S2213133715000141>. doi:<https://doi.org/10.1016/j.ascom.2015.02.003>.
- [12] R. Macfarlane, D. W. Muir, R. M. Boicourt, A. C. Kahler, III, J. L. Conlin, The NJOY Nuclear Data Processing System, Version 2016, Technical Report, Los Alamos National Laboratory, 2017. URL: <https://www.osti.gov/biblio/1338791>. doi:[10.2172/1338791](https://doi.org/10.2172/1338791).
- [13] J. Ortensi, B. A. Baker, M. P. Johnson, Y. Wang, V. M. Labouré, S. Schunert, F. N. Gleicher, M. D. DeHart, Validation of the griffin application for treat transient modeling and simulation, Nuclear Engineering and Design 385 (2021) 111478. URL: <https://www.sciencedirect.com/science/article/pii/S0029549321004301>. doi:<https://doi.org/10.1016/j.nucengdes.2021.111478>.
- [14] J. Ortensi, B. Baker, Y. Wang, V. Labouré, M. DeHart, Simulation of transient prescription measurements in treat using mammoth, Tech. Rep. INL/EXT-18-51389, Idaho National Laboratory (2018).

- [15] C. Lee, W. S. Yang, Mc2-3: Multigroup cross section generation code for fast reactor analysis, Nuclear Science and Engineering 187 (2017) 268–290. URL: <https://doi.org/10.1080/00295639.2017.1320893>. doi:10.1080/00295639.2017.1320893. arXiv:<https://doi.org/10.1080/00295639.2017.1320893>.
- [16] Y. Jung, C. Lee, PROTEUS-MOC User Manual, Technical Report ANL/NE-18/10, Argonne National Laboratory, 2018.
- [17] Idaho National Laboratory, Idaho’s third supercomputer coming to collaborative computing center, 2020. Online, <https://inl.gov/national-homeland-security/idahos-third-supercomputer-coming-to-collaborative-computing-center/>.
- [18] D. W. Nigg, K. A. Steuhm, Advanced Test Reactor Core Modeling Update Project Annual Report for Fiscal Year 2012, Technical Report INL/EXT-12-27059, Idaho National Laboratory, 2012. doi:10.2172/1060998.
- [19] M. Chadwick, P. Obložinský, M. Herman, et al., ENDF/B-VII.0: Next generation evaluated nuclear data library for nuclear science and technology, Nuclear Data Sheets 107 (2006) 2931–3118. URL: <https://www.sciencedirect.com/science/journal/00903752>. doi:10.1016/j.nds.2006.11.001.
- [20] VTT Finland, 2017. Online, https://serpent.vtt.fi/mediawiki/index.php/CASMO_18-group_structure.
- [21] VTT Finland, 2017. Online, https://serpent.vtt.fi/mediawiki/index.php/Pre-defined_energy_group_structures.
- [22] J. Ortensi, Y. Wang, A. Laurier, S. Schunert, A. Hébert, M. DeHart, A newton solution for the superhomogenization method: The PJFNK-SPH, Annals of Nuclear Energy 111 (January 2018) 579–594.

Revised PDF with changes highlighted